Determination of fine magnetic structure of magnetic multilayer with quasi antiferromagnetic layer by using polarized neutron reflectivity analysis

Cite as: AIP Advances **10**, 015323 (2020); https://doi.org/10.1063/1.5130445
Submitted: 03 October 2019 . Accepted: 27 December 2019 . Published Online: 16 January 2020

Yongshi Zhong, Yuichiro Kurokawa, Gen Nagashima, Shu Horiike, Takayasu Hanashima, Daniel Schönke, Pascal Krautscheid, Robert M. Reeve, Mathias Kläui, and Hiromi Yuasa

Determination of fine magnetic structure of magnetic multilayer with quasi antiferromagnetic layer by using polarized neutron reflectivity analysis

Cite as: AIP Advances 10, 015323 (2020); doi: 10.1063/1.5130445
Presented: 5 November 2019 • Submitted: 3 October 2019 •
Accepted: 27 December 2019 • Published Online: 16 January 2020

Yongshi Zhong,[1] Yuichiro Kurokawa,[1] Gen Nagashima,[1] Shu Horiike,[1] Takayasu Hanashima,[2] Daniel Schönke,[3] Pascal Krautscheid,[3] Robert M. Reeve,[3] Mathias Kläui,[3] and Hiromi Yuasa[1,a)]

AFFILIATIONS

[1]Faculty of Information Science and Electrical Engineering, Kyushu University, Fukuoka 819-0395, Japan
[2]Neutron Science and Technology Center, CROSS, Tokai 319-1106, Japan
[3]Institute of Physics, Johannes Gutenberg-University Mainz, 55099 Mainz, Germany

Note: This paper was presented at the 64th Annual Conference on Magnetism and Magnetic Materials.
[a)]**Email:** hiromi.yuasa@ed.kyushu-u.ac.jp

ABSTRACT

We carried out polarized neutron reflectivity (PNR) analysis to determine the fine magnetic structure of magnetic multilayers with quasi-antiferromagnetic (quasi-AFM) layers realized by 90-deg coupling using two $Co_{90}Fe_{10}$ layers, and quantitatively evaluated the magnetization of quasi-AFM layers. Two types of samples with different buffer layers, Ru buffer and a NiFeCr buffer, were investigated and the average angles between the respective magnetization of the two $Co_{90}Fe_{10}$ layers were estimated to be +/− 39 degrees and +/− 53 degrees. In addition, less roughness was found in the NiFeCr buffer sample resulting stronger 90-deg coupling. A perfect quasi-AFM is expected to be realized by a flat interface of the magnetic multilayer.

Antiferromagnetic (AFM) spintronics had attracted increasing attention in the past few years owing to the different properties and potentials compared to ferromagnetic (FM) spintronics such as high resonance frequencies and a zero stray field.[1–4] It is well known that spin torque oscillation (STO) can be observed in FM materials with ease, but there are also dipolar interactions resulting in leakage of the magnetic field which is disadvantageous for STO applications like magnetoresistive random access memory (MRAM).[5] AFM materials, however, do not have magnetic field leakage as they exhibit alternating antiparallel magnetic moments. This characteristic is useful in device design because the stray field can be neglected. Although theoretical spin transfer torque (STT) in AFM materials has been reported[1,6,7] and experimentally observed,[6–14] obvious and practical STO has not yet been directly obtained because of the strong exchange coupling between adjacent atoms. To realize STO without a stray field, we successfully created a new type of magnetic material, named a quasi-AFM layer, whose magnetic domains are alternating antiparallel.[15] STO is expected to be observed in quasi-AFM layer because it exhibits FM coupling within one domain and each magnetic moment can oscillate simultaneously. In addition, zero stray fields can be realized owing to the alternating antiparallel magnetization in the next magnetic domains. The magnetic behavior of quasi-AFM is considered an intermediate state between FM and AFM materials.

The quasi-AFM layer is realized by 90-deg coupling, an interlayer exchange interaction between two FM layers separated by a thin layer.[15–37] The magnetic coupling energy E of the magnetic multilayer can be explained by the following equation if the quadratic term is considered:[15–36]

$$E = -A_{12}(\boldsymbol{M}_1 \cdot \boldsymbol{M}_2) - B_{12}(\boldsymbol{M}_1 \cdot \boldsymbol{M}_2)^2, \quad (1)$$

where $\boldsymbol{M_1}$ and $\boldsymbol{M_2}$ are the unit magnetization in the first and second FM layers respectively, and A_{12} and B_{12} are the bilinear and biquadratic coupling coefficients, respectively. Equation (1) can be converted to:

$$E \propto -B_{12}\cos\theta(\cos\theta + \frac{A_{12}}{B_{12}}), \tag{2}$$

where θ is the angle between the magnetization of the two FM layers, as shown in Fig. 1(a). When $|A_{12}| < 2|B_{12}|$ and $B_{12} < 0$, $\boldsymbol{M_1}$ and $\boldsymbol{M_2}$ should take up an intermediate orientation in an angle between 0° and 180°, i.e., 90-deg coupling. When the magnetization in the first FM layer is fixed in one direction, the magnetization in the second FM layer should be alternating antiparallel because of the 90-deg coupling energy and the magnetostatic energy. Thus, we successfully fabricated a quasi-AFM layer. To utilize the unique quasi-AFM layer as a tunable material between FM and AFM, it is important to understand the fine magnetic structure corresponding to the magnetic process. Therefore, in this study, we carried out polarized neutron reflectivity (PNR) analysis of the multilayer with quasi-AFM layers because PNR is suitable for analyzing the magnetization quantitively and obtaining 3D information of multilayers.[38,39] Additionally, PNR makes it possible to understand the magnetization dependence on the external fields.

Two types of multilayer films with different buffer layers, Ru buffer and NiFeCr buffer, were grown on thermally oxidized Si wafers by sputtering, as shown in Figs. 1(b) and (c), respectively. The magnetization of $Co_{90}Fe10$ (A) was fixed in the $+x$-direction by IrMn, and there was 90-deg coupling between $Co_{90}Fe_{10}$ (A) and $Co_{90}Fe_{10}$ (B) through Fe–O. As a result, $Co_{90}Fe_{10}$ (B) became the quasi-AFM layer, which was macroscopically confirmed by magnetic hysteresis (MH) curves Direct observation using scanning electron microscopy with polarization analysis (SEMPA)[40,41] indicated that $Co_{90}Fe_{10}$ (B) had imperfect 90 degrees magnetization with respect to the magnetization of $Co_{90}Fe_{10}$ (A).[15]

To obtain more accurate magnetization information for the two types of multilayer films, we carried out PNR measurements using a neutron wavelength of 0.24–0.88 nm at SHARAKU (BL17) in the Materials and Life Science Experimental Facility (MLF), Japan Proton Accelerator Research Complex (J-PARC).[42,43] PNR depends on the nuclear coherent scattering length and the magnetic-scattering length density profile, which is useful for analyzing crystal structure and magnetic structure simultaneously. The reflectivity was measured as a function of wave-vector transfer.[38,39]

$$Q = 4\pi\sin(\Theta)/\lambda \tag{3}$$

where Θ and λ are the angles of incidence and wavelength of neutron, respectively. PNR consists of two types of measurements, the reflected neutrons with the same polarization, i.e., non-spin-flip, (R++ and R−−), and the reflected neutrons with polarizations opposite the incident polarization, i.e., spin-flip, (R+− and R−+). R++ and R−− refer to the parallel and antiparallel between neutron spin polarization and the sample polarization, respectively. R+− and R−+ refer to the verticality of neutron spin polarization and the sample polarization, respectively. In our experiment, the sample size was 20 mm × 20 mm in the x-y plane and the neutron beam was irradiated along the x-axis with changing incident angle Θ at room temperature (RT), as shown in Fig. 1(d). The wave-vector transfer Q ranged from 0.07 to 3.5nm^{-1}. The applied magnetic fields along the x-axis were +1000 Oe, +29 Oe, and −28 Oe for Ru buffer sample; and +1000 Oe, +32 Oe, and −45 Oe for the NiFeCr buffer sample. The correction for the polarization efficiencies was applied for the non-spin-flip reflectivity and the spin-flip reflectivity. As there are too many fitting parameters to fit correctively, X-ray reflectivity (XRR) analysis was carried out to decide the structure parameters, i.e., thickness, atomic density and roughness of each layer. The data reduction software Utsusemi[44] in BL17 was applied for conversion from the data to the polarized reflectivity, and GenX was used for the PNR analysis.[45] In GenX, the figure of merit (FOM) is the indication of the consistency of the fitting curve and experimental data. We could obtain the reasonable results after XRR and PNR fittings were repeated alternately until the FOM was less than 2e^{-1}.

Figures 2(a) and (b) show the PNR profiles and fitting curves for the Ru and NiFeCr buffer samples, respectively, when the applied

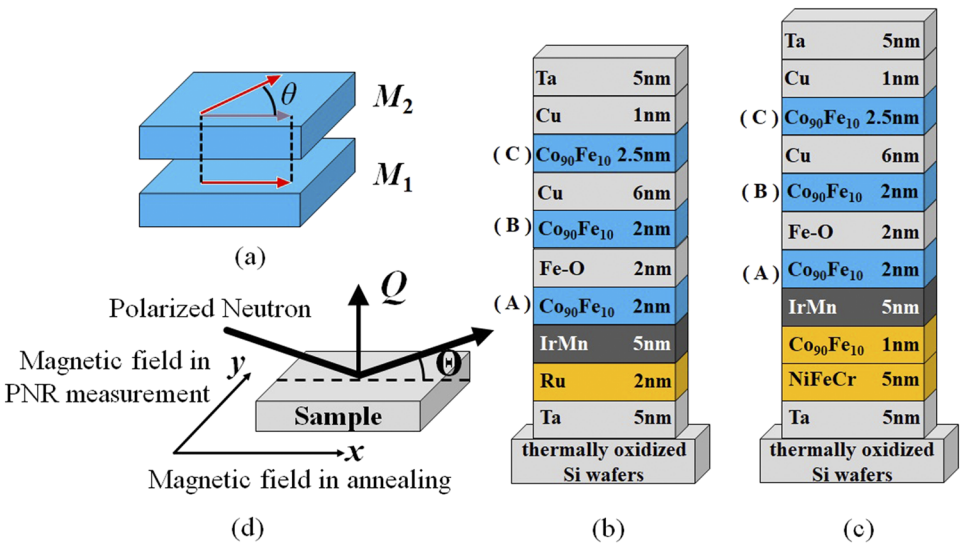

FIG. 1. Angle θ between magnetization of the two FM layers (a). Sample structures with Ru buffer sample (b) and NiFeCr buffer sample (c). PNR measurement layout and Cartesian coordination definition (d).

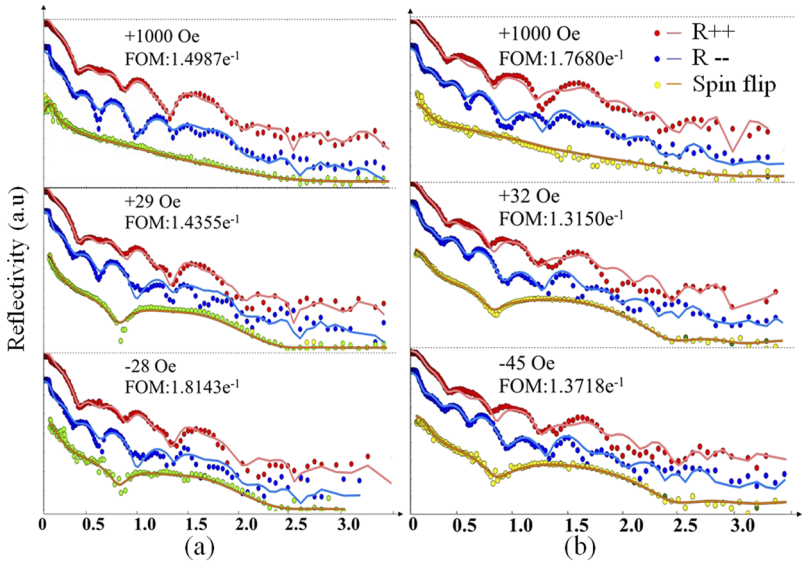

FIG. 2. PNR results and fitting curves; (a) Ru buffer sample in +1000 Oe, +29 Oe, −28 Oe and, (b) NiFeCr buffer sample in +1000 Oe, +32 Oe, −45 Oe.

fields are changed. The dots indicate the experimental data and the lines show the calculated results of fitting. After repeating the XRR and PNR fitting, we obtain sufficiently good agreement between the experimental data and the calculated data with FOM less than $2e^{-1}$. The fitting results of the parameters of each layer are summarized in Table I. Regarding the Fe–O layer, we tried various combinations of FeO, Fe_3O_4, and Fe_2O_3. Finally, the calculated curve of the FeO/Fe_2O_3 bilayer showed the best agreement with the experimental data. The structure parameters did not change when the external fields were changed, indicating that the fitting results were reasonable. In addition, the magnetic structure parameters were widely changed by the applied field. To clarify the magnetic structure, we

TABLE I. The structure parameters and the magnetic structure parameters derived from PNR analysis for the Ru and NiFeCr buffer samples.

	Ru buffer sample						NiFeCr buffer sample					
	Thickness /nm	Density /g cm^{-3}	Roughness /nm	Magnetization +1000 Oe	+29 Oe	-28 Oe	Thickness /nm	Density /g cm^{-3}	Roughness /nm	Magnetization +1000 Oe	+32 Oe	-45 Oe
Ta_2O_5	2.69	9.17	0.81				3.33	8.88	0.30			
Ta	2.50	15.92	0.60				2.43	16.53	0.02			
Cu	0.80	9.45	0.40				0.70	8.02	0.49			
$Co_{90}Fe_{10}$(C)	2.20	9.54	1.10	1.90 μB 90 deg	1.90 μB 85 deg	1.90 μB -84 deg	2.80	9.64	0.50	1.80 μB 89 deg	1.90 μB 88 deg	1.83 μB -90 deg
Cu	5.49	8.97	0.50				5.56	8.02	0.50			
$Co_{90}Fe_{10}$(B)	1.98	7.79	0.40	1.78 μB 91 deg	1.42 μB 1 deg	1.41 μB 0 deg	2.00	9.63	0.25	1.78 μB 92 deg	1.10 μB 1 deg	1.12μB -19 deg
Fe_2O_3	1.00	2.61	0.50				1.71	2.65	0.01			
FeO	0.95	4.18	0.70				0.10	5.17	0.02			
$Co_{90}Fe_{10}$(A)	1.97	9.54	0.30	1.90 μB 51 deg	1.90 μB 1 deg	1.90 μB 0 deg	1.91	9.64	0.33	1.90 μB 63 deg	1.78 μB 3 deg	1.75 μB -28 deg
$Ir_{22}Mn_{78}$	5.56	11.59	0.50				5.19	11.58	0.13			
$Co_{90}Fe_{10}$							1.18	9.54	0.15			
Ru or $Ni_{48}Fe_{22}Cr_{40}$	2.10	14.10	0.60				4.71	7.21	0.42			
Ta	5.20	14.72	0.27				4.77	15.02	0.14			
SiO_2	200	2.10	0.32				204	1.80	0.01			

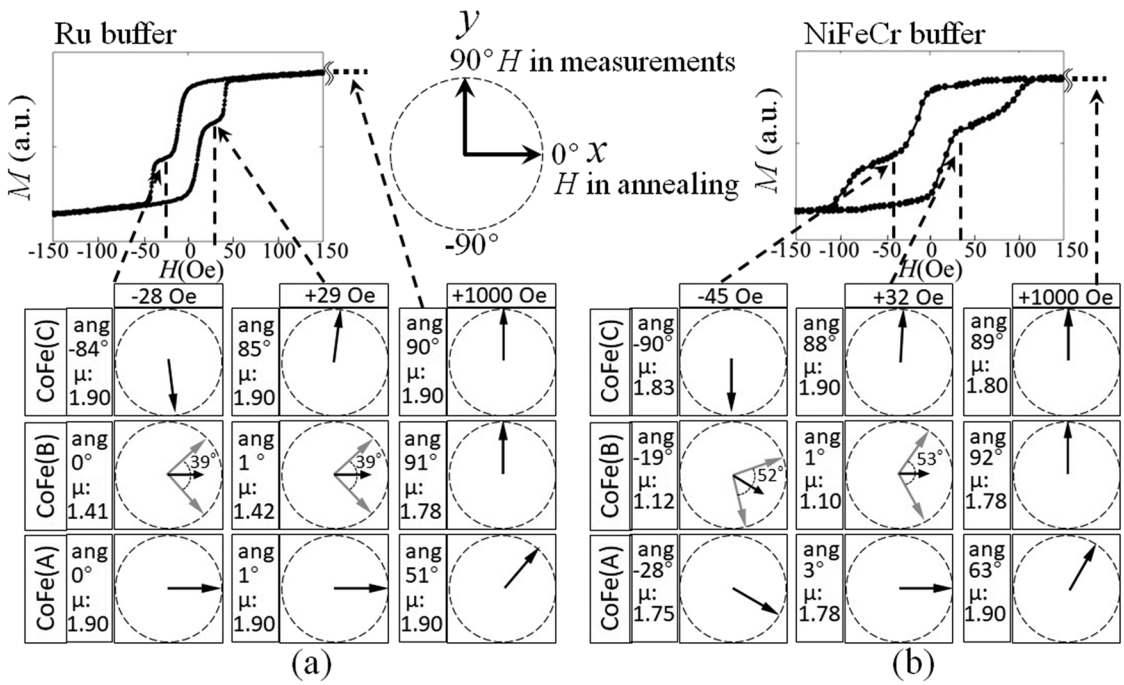

FIG. 3. Correspondence between MH curves and schematic images of magnetization for $Co_{90}Fe_{10}$ (A), $Co_{90}Fe_{10}$ (B) and $Co_{90}Fe_{10}$ (C) estimated from PNR analysis for (a) Ru and (b) NiFeCr buffer samples.

represent the magnetization images of $Co_{90}Fe_{10}$(A), (B), and (C) in Fig. 3.

Figures 3(a) and (b) show the correspondence between the MH curves and the magnetic configurations of $Co_{90}Fe_{10}$ (A), $Co_{90}Fe_{10}$ (B), and $Co_{90}Fe_{10}$ (C) estimated from PNR fitting for the Ru buffer sample and NiFeCr buffer samples, respectively. The magnetic field was applied in the PNR measurement along the y-axis which is normal to the biasing field of $Co_{90}Fe_{10}$ (A) from IrMn along the x-axis. Here, if the $Co_{90}Fe_{10}$ (A) magnetization is perfectly fixed in the $+x$-direction by IrMn, the $+x$-directions corresponds to $\theta = 0^\circ$, and the $+y$ and $-y$ direction correspond to $\theta = 90^\circ$ and $\theta = -90^\circ$, respectively.

First, let us focus on the PNR results of the $Co_{90}Fe_{10}$ (C) layer in the two samples, in which the magnetization is expected to be free to reverse. At +1000 Oe, the magnetization for the Ru and NiFeCr buffer samples was 1.90μ_B, 90° and 1.90μ_B, 89°, respectively, which means that the magnetization saturated in the applied field direction, the $+y$-direction. When the applied field H_y for the Ru and NiFeCr buffer samples was changed from +29 Oe to −28 Oe and from +32 Oe to −45 Oe, respectively, the magnetization changed from 1.90μ_B, 85° and 1.90μ_B, 88° to 1.90μ_B, −84° and 1.83μ_B, −90°, respectively. These results mean that the magnetization reversed as expected.

Second, let us see the PNR results of the $Co_{90}Fe_{10}$ (A) layer in both samples, in which the magnetization is expected to be fixed in the $+x$-direction in a low applied field. At +1000 Oe, the magnetization was 1.90μ_B, 51° and 1.90μ_B, 63° for the Ru and NiFeCr buffer samples, respectively. These results are attributed to the competition of the exchange bias in the direction of the x-axis by the IrMn layer and the external field H_y in the direction of the y-axis. As the applied field decreased to +29 Oe and +32 Oe, the magnetization of $Co_{90}Fe_{10}$ (A) recovered in the x-direction as expected. As the applied field swept to the negative value, the magnetization of the $Co_{90}Fe_{10}$ (A) layer for the NiFeCr buffer sample tilted toward −28°, whereas while that for the Ru buffer sample stayed the same, which corresponds to the fact that the exchange bias from IrMn for the NiFeCr buffer sample was weaker than that of the Ru buffer sample.[15]

Finally, let us consider the PNR results of the $Co_{90}Fe_{10}$ (B) layer, which is expected to be the quasi-AFM layer. At +1000 Oe, the magnetization was 1.78μ_B, 91° and 1.78μ_B, 92° for the Ru and NiFeCr buffer samples, respectively, meaning that the magnetization saturated in the applied field direction. At +29 Oe and +32 Oe, the magnetization was 1.42μ_B, 1° and 1.10μ_B, 1° for the Ru and NiFeCr buffer samples, respectively. At −28 Oe and −45 Oe, the magnetization was 1.41μ_B, 0° and 1.12μ_B, −19°, respectively. From these results, we derived the images of magnetization of $Co_{90}Fe_{10}$ (B) quantitively as explained below.

We consider the Ru buffer sample first. The magnetization of 1.42μ_B is evidently lower than the saturated moment 1.82μ_B, which means a part of the magnetization of $Co_{90}Fe_{10}$ (B) in the low field was canceled out due to the antiparallel magnetization originating from the 90-deg coupling with $Co_{90}Fe_{10}$ (A). From the energy Eq. (3), the magnetization of $Co_{90}Fe_{10}$ (A) and $Co_{90}Fe_{10}$ (B) should be at angle θ. In the +29 Oe field, because the magnetization of $Co_{90}Fe_{10}$ (A) was 1.90μ_B, 1°, the magnetization angle of $Co_{90}Fe_{10}$ (B) should be 1° + θ or 1° − θ to satisfy the smallest magnetic static energy. Because the magnetization with an angle of 1° + θ can be decomposed into the $+y$-direction and the $+x$-direction, whereas the magnetization with an angle of 1° − θ can be decomposed into the $-y$-direction and the $+x$-direction, the components of magnetization

in the $+y$-direction and the $-y$-direction will be canceled out. As a result, only the magnetization in the $+x$-direction can be observed. If $\theta = 90°$, which means a perfect 90-deg coupling, we cannot detect the magnetization of $Co_{90}Fe_{10}$ (B) at all by PNR. After the above consideration, we derived the average angle between the magnetization of $Co_{90}Fe_{10}$ (A) and $Co_{90}Fe_{10}$ (B). This angle was estimated to be +/− 39° from $\cos^{-1}(1.42\mu_B/1.82\mu_B)$, as shown in Fig. 3. The magnetization of $Co_{90}Fe_{10}$ (B) at −28 Oe can also be explained in this way. The magnetization of $Co_{90}Fe_{10}$ (A) and $Co_{90}Fe_{10}$ (B) was also estimated to be +/− 39°. These results indicate that the magnetization of $Co_{90}Fe_{10}$ (B) was not completely alternating antiparallel, which well agreed with the SEMPA image of the $Co_{90}Fe_{10}$ (B) layer and magnetization derived from the MH curves.[15]

The magnetization of the $Co_{90}Fe_{10}$ (B) layer for the NiFeCr buffer sample can be explained in the same way. The average angle between the magnetization of $Co_{90}Fe_{10}$ (A) and $Co_{90}Fe_{10}$ (B) at +32 Oe was estimated to be +/− 53° from $\cos^{-1}(1.10\mu_B/1.82\mu_B)$. The magnetization of the $Co_{90}Fe_{10}$ (B) layer at −45 Oe was $1.12\mu_B$, −19°, which considered to be the combined effect of 90-deg coupling and the magnetic field, and the magnetization had begun to reverse. The average angle between the magnetization of $Co_{90}Fe_{10}$ (A) and $Co_{90}Fe_{10}$ (B) at −45 Oe was estimated to be +/− 52° from $\cos^{-1}(1.12\mu_B/1.82\mu_B)$.

The average rotation angle θ of the NiFeCr buffer sample was bigger than that of the Ru buffer sample, which means the 90-deg coupling of the NiFeCr buffer sample was larger than that of the Ru buffer sample, which is considered to be the effect of roughness. As shown in Table I, the Ru buffer sample had greater roughness than the NiFeCr buffer sample. The greater roughness will reinforce the orange-peel ferromagnetic coupling,[46,47] which breaks the necessary condition of the energy balance between ferromagnetic and antiferromagnetic coupling to realize 90-deg coupling. This greater roughness in the Ru buffer sample can also be observed from the high-resolution cross-sectional TEM images in Ref. 15.

In conclusion, we successfully determined the magnetic structure of multilayers with quasi-AFM layers made by 90-deg coupling through Fe–O on Ru and NiFeCr buffers, by using PNR analysis. The average angle between the magnetization of the two $Co_{90}Fe_{10}$ layers was estimated to be +/− 39° and +/− 53° for the Ru and NiFeCr buffer samples, respectively, which is explained by the roughness of Fe–O between the two $Co_{90}Fe_{10}$ layers. A quasi-AFM layer with perfectly antiparallel magnetization is expected to be realized as the flattening Fe–O layer.

This work was supported by the Canon Foundation, the JSPS Program for Fostering Globally Talented Researchers, and JSPS KAKENHI Grant Number JP19K04471. The neutron experiment was carried out in Materials and Life Science Experimental Facility (MLF), Japan Proton Accelerator Research Complex (J-PARC) and user program proposal No. 2018B0182.

REFERENCES

[1] A. H. MacDonald and M. Tsoi, Phil. Trans., R. Soc. A **369**, 3098 (2011).
[2] R. Duine, Nature Mater **10**, 344 (2011).
[3] T. Jungwirth, X. Marti, P. Wadley, and J. Wunderlich, Nature Nanotechnology **11**, 231 (2016).
[4] R. Khymyn, I. Lisenkov, V. Tiberkevich, B. A. Ivanov, and A. Slavin, Scientific Report **7**, 43705 (2017).
[5] R. Sbiaa, H. Meng, and S. N. Piramanayagam, Phys. Status Solidi RRL **7**, 332 (2013).
[6] A. S. Núñez, R. A. Duine, P. Haney, and A. H. MacDonald, Phys. Rev. B **73**, 214426 (2006).
[7] Z. Wei, A. Sharma, A. S. Nunez, P. M. Haney, R. A. Duine, J. Bass, A. H. MacDonald, and M. Tsoi, Phys. Rev. Lett. **98**, 116603 (2007).
[8] S. Urazhdin and N. Anthony, Phys. Rev. Lett. **99**, 046602 (2007).
[9] P. M. Haney and A. H. MacDonald, Phys. Rev. Lett. **100**, 196801 (2008).
[10] Z. Wei, A. Sharma, A. S. Nunez, P. M. Haney, R. A. Duine, J. Bass, A. H. MacDonald, and M. Tsoi, Phys. Rev. Lett. **98**, 116603 (2007).
[11] Z. Wei, J. Basset, A. Sharma, J. Bass, and M. Tsoi, Appl. Phys. **105**, 07D108 (2009).
[12] T. Moriyama, S. Takei, M. Nagata, Y. Yoshimura, N. Matsuzaki, T. Terashima, Y. Tserkovnyak, and T. Ono, Appl. Phys. Lett. **106**, 162406 (2015).
[13] T. Moriyama, M. Kamiya, K. Oda, K. Tanaka, K.-J. Kim, and T. Ono, Phys. Rev. Lett. **119**, 267204 (2017).
[14] X. Z. Chen, R. Zarzuela, J. Zhang, C. Song, X. F. Zhou, G. Y. Shi, F. Li, H. A. Zhou, W. J. Jiang, F. Pan, and Y. Tserkovnyak, Phys. Rev. Lett. **120**, 207204 (2018).
[15] G. Nagashima, Y. Kurokawa, Y. Zhong, S. Horiike, D. Schönke, P. Krautscheid, R. Reeve, M. Kläui, Y. Inagaki, T. Kawae, T. Tanaka, K. Matsuyama, K. Ohnishi, T. Kimura, and H. Yuasa, J. Appl. Phys. **126**, 093901 (2019).
[16] J. C. Slonczewski, Phys. Rev. Lett. **67**, 3172 (1991).
[17] M. Ruhrig, R. Schafer, A. Hubert, R. Mosler, J. A. Wolf, S. Demokritov, and P. Grünberg, Phys. Status. Solidi. (a) **125**, 635 (1991).
[18] B. Heinrich, J. F. Cochran, M. Kowalewski, J. Kirschner, Z. Celinski, A. S. Arrott, and K. Myrtle, Phys. Rev. B **44**, 9348 (1991).
[19] J. Unguris, R. J. Celotta, and D. T. Pierce, Phys. Rev. Lett. **67**, 140 (1991).
[20] A. Fuss, S. Demokritov, P. Grünberg, and W. Zinn, J. Magn. Magn. Mater. **103**, L221 (1992).
[21] C. J. Gutierrez, J. J. Krebs, M. E. Flipkowski, and G. A. Prinz, J. Magn. Magn. Mater. **116**, L305 (1992).
[22] B. Heinrich, Z. Celinski, J. F. Cochran, A. S. Arrott, K. Myrtle, and S. T. Purcell, Phys. Rev. B **47**, 5077 (1993).
[23] B. Rodmacq, K. Dumesnil, P. Mangin, and M. Hennion, Phys. Rev. B **48**, 3556 (1993).
[24] J. C. Slonczewski, J. Appl. Phys. **73**, 5957 (1993).
[25] M. E. Filipkowski, J. J. Krebs, G. A. Prinz, and C. J. Gutierrez, Phys. Rev. Lett. **75**, 1847 (1995).
[26] J. C. Slonczewski, J. Magn Magn. Mater. **150**, 13 (1995).
[27] S. O. Demokritov, J. Phys. D: Appl. Phys. **31**, 925 (1998).
[28] P. A. A. van der Heijden, C. H. W. Swüste, W. J. M. de Jonge, J. M. Gaines, J. T. W. M. van Eemeren, and K. M. Schep, Phys. Rev. Lett. **82**, 1020 (1999).
[29] S.-S. Yana, P. Grünberg, and L.-M. Mei, J. Appl. Phys. **88**, 983 (2000).
[30] H. Fukuzawa, K. Koi, H. Tomita, H. N. Fuke, H. Iwasaki, and M. Sahashi, J. Appl. Phys. **91**, 6684 (2002).
[31] C.-H. Lai and K. H. Lu, J. Appl. Phys. **93**, 8412 (2003).
[32] S. Maat and B. A. Gurney, J. Appl. Phys. **93**, 7229 (2003).
[33] C. H. Lai and K. H. Lu, J. Appl. Phys. **93**, 8412 (2003).
[34] H. Wang, A. Sato, K. Saito, S. Mitani, K. Takanashi, and K. Yakushiji, Appl. Phys. Lett. **90**, 142510 (2007).
[35] T. Jungwirth, X. Marti, P. Wadley, and J. Wunderlich, Nature Nanotechnology. **11**, 231 (2016).
[36] K. Koike, H. Matsuyama, H. Todokoro, and K. Hayakawa, Jpn. J. Appl. Phys. **24**, 1078 (1985).
[37] A. I. Morosov and A. S. Sigov, Phys. Solid State **54**(2), 219–242 (2012).
[38] T. Chatterji, "Neutron scattering from magnetic materials," in *Polarized Neutron Reflectometry*, edited by C. F. Majkrzak, K. V. O'Donovan, and N. F. Berk (Elsevier, 2006), Chapter 9.
[39] H. Hayashida, T. Oku, H. Kira, K. Sakai, M. Takeda, Y. Sakaguchi, T. Ino, T. Shinohara, K. Ohoyama, J. Suzuki, K. Kakurai, M. Mizusawa, N. Miyata, D. Yamazaki, R. Maruyama, K. Soyama, and M. Arai, J. Phys: Conference Series **528**(1), 012020 (2014).

[40]K. Koike, H. Matsuyama, H. Todokoro, and K. Hayakawa, J. Appl. Phys. **24**, 1078 (1985).
[41]J. Unguris, G. Hembree, R. J. Celotta, and D. T. Pierce, J. Magn Magn. Mater. **54**, 1629 (1986).
[42]Y. Inamura, T. Nakatani, J. Suzuki, and T. Otomo, J. Phys. Soc. Japan **82**, SA031 (2013).
[43]M. Takeda, D. Yamazaki, K. Soyama, R. Maruyama, H. Hayashida, H. Asaoka, T. Yamazaki, M. Kubota, K. Aizawa, M. Ara, Y. Inamura, T. Itoh, K. Kanekoi, T. Nakamura, T. Nakatani, K. Oikawa, T. Ohhara, Y. Sakaguchi, K. Sakasai, T. Shinohara, J. Suzuki, K. Suzuya, I. Tamura, K. Toh, H. Yamagishi, N. Yoshida, and T. Hirano, Chinese J. Phys. **50**, 161 (2012).
[44]K. Sakasai, S. Satoh, T. Seya, T. Nakamura, K. Toh, H. Yamagishi, K. Soyama, D. Yamazaki, R. Maruyama, T. Oku, T. Ino, H. Kira, H. Hayashida, K. Sakai, S. Itoh, K. Suzuya, W. Kambara, R. Kajimoto, K. Nakajima, K. Shibata, M. Nakamura, T. Otomo, T. Nakatani, Y. Inamura, J. Suzuki, T. Ito, N. Okazaki, K. Moriyama, K. Aizawa, S. Ohira-Kawamura, and M. Watanabe, Quantum Beam Sci. **1**, 10 (2017).
[45]M. Björck and G. Andersson, J. Appl. Cryst **40**, 1174 (2007).
[46]J. C. S. Kools, W. K. Mauri, and T. Lin, J. Appl. Phys. **85**, 4466 (1999).
[47]B. D. Schrag, A. Anguelouch, S. Ingvarsson, G. X. Y. Lu, P. L. Trouilloud, A. Gupta, R. A. Wanner, W. J. Gallagher, P. M. Rice, and S. S. P. Parkin, Appl. Phys. Lett. **77**, 2373 (2000).